This article has been accepted for publication in a future issue of this journal, but has not been fully edited. Content may change prior to final publication. Citation information: DOI 10.1109/TSG.2017.2772224, IEEE Transactions on Smart Grid

Small Signal Stability Analysis of Distribution Networks with Electric Springs

Diptargha Chakravorty, *Student Member, IEEE,* Jinrui Guo, *Student Member, IEEE,* Balarko Chaudhuri, *Senior Member, IEEE,* and Shu Yuen Ron Hui, *Fellow, IEEE*

***Abstract*—This paper presents small signal stability analysis of distribution networks with electric springs (ESs) installed at the customer supply points. The focus is on ESs with reactive compensation only. Vector control of ES with reactive compensation is reported for the first time to ensure compatibility with the standard stability models of other components such as the interface inverter of distributed generators (DGs). A linearized state-space model of the distribution network with multiple ESs is developed which is extendible to include inverter-interfaced DGs, energy storage, active loads etc. The impact of distance of an ES from the substation, proximity between adjacent ESs and the R/X ratio of the network on the small signal stability of the system is analyzed and compared against the case with equivalent DG inverters. The collective operation of ESs is validated through simulation study on a standard distribution network.**

***Index Terms*—Distributed Generation, Dynamic Model, Distribution Network, Electric Spring, Small Signal Stability, State Space, Vector Control**

I. Introduction

The concept of Electric Spring (ES) was introduced to regulate the voltage at the point of coupling (PoC) in the face of intermittency in renewable (wind, solar) power [1]. The effectiveness of ES is demonstrated through proof-of-concept experiments with laboratory prototypes [2] and simulation studies with ES installed in typical distribution networks [3]. The contributions of ES in grid frequency regulation [4], power quality improvement [5], phase imbalance mitigation [6] and resilience enhancement [7] are also reported making ES an attractive prospect in future smart grids.

An ES is a power electronic compensator that injects a controllable series voltage to decouple the loads from the feeder/supply. The loads could either be a cluster of customers (domestic/industrial) [8] or individual high power loads (heating, lighting, appliances etc.) [4]. Either way, mass installation of ES would result in a very high penetration of power electronic converters in the distribution network. Adverse interaction between the distributed generator (DG) inverters and the distribution network is known to cause small signal stability problems. This has been reported in the context of microgrids [9] and distribution networks [10]. Hence, there is a concern that large penetration of ES, often in close electric proximity, could affect the small signal stability of the distribution networks. Distributed control of multiple Electric Springs (ESs) for the purpose of voltage and/or frequency regulation has been studied previously [3], [4], [11], [12]. In these studies, an ES installed in series with a load (or cluster of loads) was represented as a controllable current or power source. However, a framework for small signal stability analysis of a distribution network with multiple electric springs is yet to be reported. As use of ES for voltage/frequency control attracts increasing attention, it is important to study the overall small signal stability of a distribution network with dense penetration of ESs under different scenarios which motivates this paper.

This work follows on from previous papers [13] & [14] on modelling and stability analysis of ES (Electric Spring with only reactive compensation (ES-Q), also termed as ES version 1 in previous papers). The dynamic model in [13] is not based on the standard vector control modelling framework. Hence, the tuning of the controller gains, unlike standard vector control [15] approach which is widely used for power electronic converters, are not based on analytical methods. Moreover, it lacks an inner current control loop which is necessary for limiting the inverter current within safe limits. However, there are unique challenges in developing vector control of ES-Q due to two important factors: (a) it has a series configuration unlike PV inverters and (b) only reactive power exchange is allowed. These two factors impose a quadrature constraint between the load current, filter capacitor current and the inverter current due to which it is not appropriate to align the d-axis with the PoC voltage (which is commonly done for shunt converters).

Based on the work done in [13], a linearized state space model is developed in [14]. However, three important limitations of [14] are: (i) the frequency domain model is not based on the vector control and hence not compatible with the standard stability model for other elements such as DG inverters etc., (ii) the paper did not report the effect of change in distribution network parameters on small signal stability and (iii) the inferences are based on the results from time-domain simulation without delving into the root cause through modal analysis. This paper addressed all these issues by proposing a way of using vector control for ES-Q which can be integrated in the stability model of a distribution network and microgrid

This work was supported in part by the Engineering and Physical Science Research Council, U.K., under the Autonomic Power Systems grant EP/I031650/1, China Scholarship Council and Imperial College London (CSC No. 201604100122) and the Hong Kong Research Grant Council under the Theme-based project T23-701/14-N.

D. Chakravorty, J. Juo, B. Chaudhuri and S. Y. R. Hui are with the Department of Electrical and Electronic Engineering, Imperial College London, London, SW7 2AZ U.K. (e-mail: d.chakravorty12@imperial.ac.uk; j.guo16@imperial.ac.uk; b.chaudhuri@imperial.ac.uk; r.hui@imperial.ac.uk). S.Y.R. Hui is also with the Department of Electrical and Electronic Engineering, The University of Hong Kong.

Supporting data is available on request: please contact cappublications@imperial.ac.uk.

This article has been accepted for publication in a future issue of this journal, but has not been fully edited. Content may change prior to final publication. Citation information: DOI 10.1109/TSG.2017.2772224, IEEE Transactions on Smart Grid

with other DG inverters. A linearized state space model of a distribution network with vector controlled ES-Q is presented for stability analysis. The state-space approach is adopted instead of the impedance-based [16], [17] approach as the latter, although simple, does not allow participation factor or mode shape analysis to identify the root cause of the stability problem.

The original contributions of this paper are as follows:

1) Vector control of ES with only reactive power compensation (ES-Q) is reported for the first time which can be integrated in the stability model of distribution networks and microgrids with other DG inverters.
2) Linearized state-space model of the distribution network with vector controlled ES-Q is developed using the Component Connection Method [18] which can be easily scaled up to include more electric springs and DG inverters.
3) The developed model is used to analyse the small signal stability of the distribution network with ES-Q and compared against the stability with equivalent penetration of DG inverters. The analysis is presented for a range of scenarios covering low- to medium voltage (LV/MV) levels and sparse rural to dense urban distribution networks.

The study reported in this paper is based on a single phase network and does not consider the switching model of the converters, voltage unbalance or harmonics and neglects the dynamics of the DC link of ES-Q (in state-space model) which would require a different modelling approach (e.g. dynamic phasor). State-space model of a three-phase ES [6] could be derived from that of a single-phase ES and is not considered separately. Henceforth, an ES with reactive power compensation (ES-Q) is simply referred to as 'Electric Spring (ES) and small signal stability is termed as just 'stability'.

II. Vector Control of Electric Spring

The configuration of an ES connected in series with a resistive-inductive (RL-type) load is shown in Fig. 1 [1]. The RL-type load is denoted by R_{NC} & L_{NC} and the corresponding voltage across it is given by V_{nc}. The ES injects a controlled series voltage V_{es} across the filter capacitance (C_f) to regulate the voltage (V_{poc}) at the point of coupling (PoC) with the supply. The equivalent inductance and resistance of rest of the network including other passive loads is denoted by L_1 and R_C, respectively. The source impedance is represented by the inductance L_g.

A. Current Control Loop

The current control loop is designed based on the dynamics of the inverter current (I_{inj}), filter capacitor voltage (V_{es}) and load current (I) which can be represented in a synchronously rotating (dq) reference frame as follows [15]:

$$L_f \frac{dI_{injd}}{dt} = V_{invd} - V_{esd} - R_f I_{injd} + \omega_0 L_f I_{injq} \quad (1)$$

$$L_f \frac{dI_{injq}}{dt} = V_{invq} - V_{esq} - R_f I_{injq} - \omega_0 L_f I_{injd} \quad (2)$$

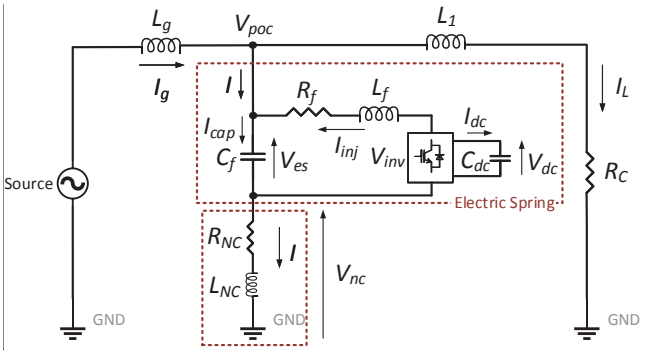

Figure 1. Electric Spring (ES) configuration

$$C_f \frac{dV_{esd}}{dt} = I_d + I_{injd} + \omega_0 C_f V_{esq} \quad (3)$$

$$C_f \frac{dV_{esq}}{dt} = I_q + I_{injq} - \omega_0 C_f V_{esd} \quad (4)$$

$$L_{NC} \frac{dI_d}{dt} = V_{pocd} - V_{esd} - R_{NC} I_d + \omega_0 L_{NC} I_q \quad (5)$$

$$L_{NC} \frac{dI_q}{dt} = V_{pocq} - V_{esq} - R_{NC} I_q - \omega_0 L_{NC} I_d \quad (6)$$

The current flowing out of the inverter (I_{inj}) is assumed to be positive. Considering I_{injd} & I_{injq} as state variables, V_{invd} & V_{invq} as control inputs and V_{esd} & V_{esq} are the disturbance inputs, the current control loop is designed following the standard method outlined in [15]. The closed loop time constant (τ) is chosen to be 0.1 ms to achieve a fast enough response while ensuring that the controller bandwidth ($\frac{1}{\tau}$) is at least 10 times smaller than the switching frequency.

B. Choice of Reference Frame (d-axis)

For regulating the point of coupling (PoC) voltage using vector control of the shunt connected inverters (such as DG inverter or STATCOM), the d-axis is normally aligned with the PoC voltage to achieve decoupled control. In this paper, the focus is on ES with only reactive power compensation (ES-Q) which injects a voltage (V_{es}) across the filter capacitor in quadrature (lead or lag) with the load current (I). In this case, aligning the $d-$axis with the PoC voltage (V_{poc}) results in non-zero inverter current (I_{inj}) on both d and q axes as shown in Fig. 2.

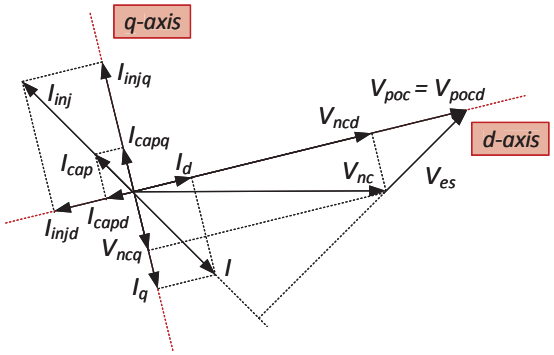

Figure 2. Phasor diagram with $d-$axis aligned with PoC voltage

This article has been accepted for publication in a future issue of this journal, but has not been fully edited. Content may change prior to final publication. Citation information: DOI 10.1109/TSG.2017.2772224, IEEE Transactions on Smart Grid

Thus, it is not possible to force the d-axis component of the inverter current to zero in order to ensure zero active power (neglecting filter and inverter losses) exchange in steady-state. To get around this problem, the d-axis could be aligned either with the filter capacitor voltage (V_{es}) or the load current (I). The latter is ruled out due to the possible implementation challenges posed by high harmonic content in the load current. So the d-axis is aligned with the filter capacitor voltage (V_{es}) as shown Fig. 3.

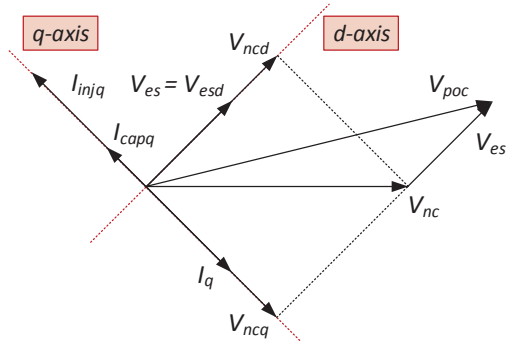

Figure 3. Phasor diagram with $d-$axis aligned with filter capacitor voltage

This enables the $d-$axis control loop to maintain the DC link voltage V_{dc} while the $q-$axis loop can be used for regulating the PoC voltage (V_{poc}) or the load voltage (V_{nc}). However, it is necessary to maintain a minimum filter capacitor voltage to allow satisfactory operation of PLL, as discussed later in Section III-B. In Fig. 3, the filter capacitor voltage (V_{es}) leads the load current (I_q) by 90° providing inductive compensation. The ES can provide capacitive compensation if V_{es} is made to lag I by 90°. The compensation mode depends on the polarity of V_{es}, unlike a STATCOM, where it is decided by the phase angle of the injected current with respect to the PoC voltage. For capacitive compensation, V_{esd} is aligned with -ve $d-$axis and I_q becomes slightly more than I_{injq} so that I_{capq} now aligns with -ve $q-$axis, thereby leading V_{esd} by 90°.

C. PoC Voltage Control Loop

The inverter current references ($I_{injdref}$ & $I_{injqref}$) are obtained from the voltage control loop described here. An approximate small-signal model for PoC voltage dynamics is presented first based on Fig. 1. The feeder resistance is neglected for simplicity in tuning the PoC control loop. The $d-$axis component of the source current can be expressed as $I_{gd} \approx I_{Ld}$ (as the $d-$axis load current component $I_d = 0$) while the $q-$axis current is given by $I_{gq} = I_{Lq} + I_q$. Assuming an ideal PLL, the PoC voltage along $d-$axis is given by (7), where the first two terms represent the *load effect* and the last term shows the *control effect*. As the current through the filter capacitor is negligibly small, an incremental change in load current is almost equal to a change in the inverter current, i.e. $\Delta I_q \approx \Delta I_{injq}$. Hence, the second term is considered as *control effect*.

$$\Delta V_{pocd} = L_g \frac{d\Delta I_{Ld}}{dt} - L_g \omega_0 \Delta I_{Lq} - L_g \omega_0 \Delta I_q \qquad (7)$$

Similarly, the $q-$axis component of the PoC voltage can be given by (8) which shows that ΔV_{pocq} depends on the rate of change of the load current.

$$\begin{aligned} \Delta V_{pocq} &= L_g \frac{d\Delta I_{gq}}{dt} + L_g \omega_0 \Delta I_{gd} \\ &= L_g \frac{d\Delta I_{Lq}}{dt} + L_g \omega_0 \Delta I_{Ld} + L_g \frac{\Delta I_q}{dt} \end{aligned} \qquad (8)$$

The voltage control loop is typically much slower than the current control loop. Hence the rate of change of small deviation in the load current ($\frac{d\Delta I_q}{dt}$) is quite small such that the effect of the small change in control variable ΔI_{injq} can be neglected in case of ΔV_{pocq}. Therefore, the control loop for the PoC voltage regulation can be represented as in Fig. 4.The current controller shown in Fig. 4 is a simple representation neglecting the feed forward and decoupling terms.

The compensator (K_{vpoc}) for the PoC voltage regulation is a proportional-integral (PI) controller with $k_{pvpoc} = 100$ and $k_{ivpoc} = 4$. The source inductance is $L_g = 0.0011$H which includes the transformer leakage and network inductance. A conservative phase margin of 90° is kept to ensure robustness in the face of varying source impedance and account for the unmodelled dynamics of the filter, loads and PLL.

D. Phase-Locked Loop (PLL)

For the single-phase PLL considered here, an additional fictitious phase was created by introducing a phase delay of $\frac{1}{4}$ of a fundamental cycle. A range of different PLL configurations have been reported [19]. However, in stability studies, the dynamics of PLL is either completely neglected [9], [20] or simplified by a proportional-integral (PI) controller [21], [22]. For a PI representation of a PLL, the tuning of k_p and k_i has little effect on the overall phase margin in the low frequency range which prompted us to adopt PI based PLL in this study. The compensator gains are chosen as $k_p = 0.3$ and $k_i = 0.5$ to allow adequate gain and phase margins at low frequencies.

E. DC Link Control Loop

The DC link control loop is designed following the standard procedure [15]. A proportional-integral compensator is used with gains $k_{pdc} = -2C_{dc}\zeta\omega$ and $k_{idc} = -C_{dc}\omega^2$, where the DC link capacitor $C_{dc} = 1.5$mF, $\zeta = 0.707$ and $\omega = 24.16$rad/s.

F. Performance Validation

The performance of the voltage control loop is tested using the system shown in Fig. 5, modelled in Matlab Simulink. The simulation model uses an average model for the converter based on a controlled voltage source on the AC side and a controlled current source on the DC side. Switching action within the converter is not modelled explicitly. The dynamics of the AC and the DC side are coupled through the ideal power balance equation i.e. $P_{ac} = P_{dc}$. A 1.8 kVA resistive load R_{new} is inserted to reduce the PoC voltage by approximately 5 V.

This article has been accepted for publication in a future issue of this journal, but has not been fully edited. Content may change prior to final publication. Citation information: DOI 10.1109/TSG.2017.2772224, IEEE Transactions on Smart Grid

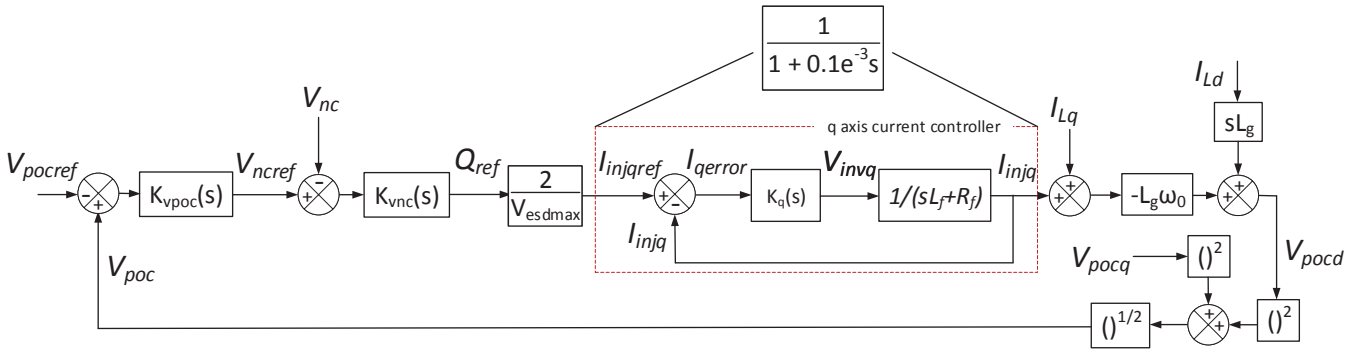

Figure 4. PoC voltage control scheme

The transformer and the feeder parameters taken from [23] correspond to typical figures for distribution networks in the UK. The R/X ratio of the lines is 4.26 (line type D in [23]) and the transformer is rated at 200 kVA.

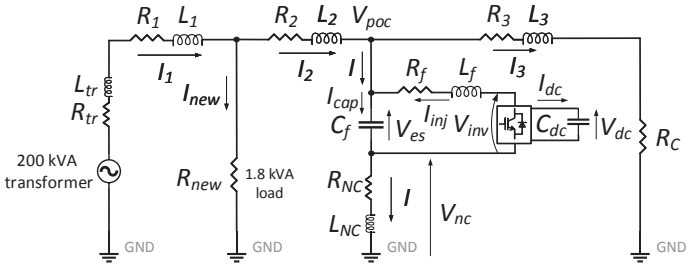

Figure 5. Test system for validation of PoC voltage controller

Electric Spring (ES) with reactive compensation does not exchange any active power between the ac and the dc side of the converter (except for supplying filter losses). To ensure this condition, the filter voltage (V_{es}) and the load current (I) always maintains a quadrature relationship. The choice of mode of operation depends on the system requirement. In case of under voltage disturbance, the ES switches from inductive to capacitive mode to provide voltage support. From the phasor diagram in Fig. 3, it is evident that in the inductive mode of operation V_{esd} is aligned with the $+d$-axis and the load current I_q is aligned with the -q-axis. In order to switch to the capacitive mode, V_{esd} needs to realign with the -d-axis while I_q needs to align with the $+q$-axis. To enable this transition process, the ES outputs a zero voltage for 3 cycles after a disturbance.

Fig. 6 shows the dynamic response following reduction in PoC voltage at t =1 s. The compensator switches from inductive mode (I lagging V_{es} by 90°) to capacitive mode (I leading V_{es} by 90°) by making the inverter current (I_{inj}) slightly less than the load current (I) such that the filter capacitor current (I_{cap}) now aligns with the negative $q-$axis. This operation can be better understood from the phasor diagram in Fig. 3.

Fig. 7(a) shows that I lags V_{es} by 90° i.e. the compensator works in inductive mode before the disturbance while after the disturbance it switches to capacitive mode where I leads V_{es} by 90° (Fig. 7(b)).

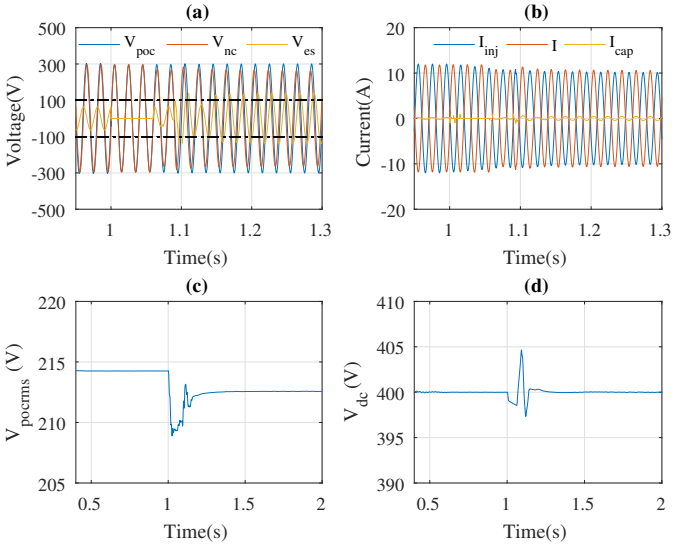

Figure 6. Dynamic response of (a) PoC, load and ES voltages; (b) inverter, load and filter capacitor current; (c) RMS value of PoC voltage and (d) DC link voltage

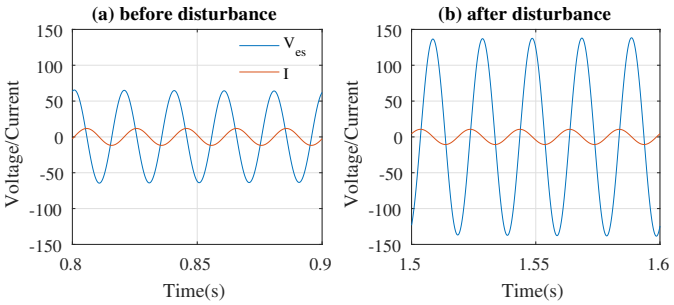

Figure 7. ES voltage (V_{es}) and load current (I) (a) before the disturbance (inductive mode) and (b) after the disturbance (capacitive mode)

From Fig. 6(c), it is clear that the PoC voltage could not be regulated at its pre-disturbance level due to violation of the inverter current limit which is set according to the allowable voltage variation across the load [11]. This limit for V_{nc} is fixed at ± 0.1 per unit in this particular case. Deviation in DC bus voltage after the disturbance, seen in Fig. 6(d), is caused by additional losses in the filter resistor (R_f) due to change in I_{inj}.

This article has been accepted for publication in a future issue of this journal, but has not been fully edited. Content may change prior to final publication. Citation information: DOI 10.1109/TSG.2017.2772224, IEEE Transactions on Smart Grid

III. Linearized State Space Model (SSM)

The linearized state-space model (SSM) of a distribution network with ES is developed here. First, the SSM is developed separately for the following sub-systems (a) PLL (b) PoC voltage control loop (c) current control loop (d) filter and (e) network and loads. Then, the Component Connection Method (CCM) [18] is used to obtain the overall SSM. For simplicity, only resistive loads are considered and the DC link dynamics is neglected.

A. PLL

The PI compensator based single phase PLL has one state variable associated with the compensator (Δx_1) and another one corresponding to the integrator ($\Delta\theta$). The input and output variables are ΔV_{esq} and $\Delta\omega$, $\Delta\theta$ where ΔV_{esq} denotes the incremental change in $q-$axis component of the filter voltage, $\Delta\omega$ denotes the change in PLL frequency and $\Delta\theta$ represents the change in PLL angle. The SSM of PLL is given by (9) and (10) where k_p and k_i are proportional and integral gains, respectively.

$$\begin{bmatrix}\Delta\dot{x_1}\\ \Delta\dot{\theta}\end{bmatrix} = \begin{bmatrix}0 & 0\\ k_i & 0\end{bmatrix}\begin{bmatrix}\Delta x_1\\ \Delta\theta\end{bmatrix} + \begin{bmatrix}1\\ k_p\end{bmatrix}\begin{bmatrix}\Delta V_{esq}\end{bmatrix} \tag{9}$$

$$\begin{bmatrix}\Delta\omega\\ \Delta\theta\end{bmatrix} = \begin{bmatrix}k_i & 0\\ 0 & 1\end{bmatrix}\begin{bmatrix}\Delta x_1\\ \Delta\theta\end{bmatrix} + \begin{bmatrix}k_p\\ 0\end{bmatrix}\begin{bmatrix}\Delta V_{esq}\end{bmatrix} \tag{10}$$

B. PoC Voltage Control Loop

The block diagram of the voltage control loop is shown in Fig. 8 which is divided into: outer PI controller (Fig. 8 (a)) and inner integral controller (Fig. 8 (b)). The state variable associated with the outer loop is denoted by Δx_{21}. The input signal V_{pocmag} is the measured PoC voltage which can be expressed in terms of $dq-$components as $\sqrt{V_{pocd}^2 + V_{pocq}^2}$. This non-linear term has been linearized about a stable operating point $V_{pocmag0}$ which results in $(\frac{V_{pocd0}}{V_{pocmag0}}\Delta V_{pocd})$ for an incremental change in $d-$ axis component. Similar expression can be obtained for an incremental change in the $q-$axis component. Thus, the SSM of the outer loop (Fig. 8 (a)) is given by (11) and (12). k_{pv} and k_{iv} are the proportional and integral gains of the voltage control loop compensator, respectively. In Fig. 8 (a) the symbol for the sum is considered $-V_{pocmagref} + V_{pocmag}$ based on the operating principle of electric spring. An increase in PoC voltage magnitude (due to disturbance) results in a positive error thus increasing the voltage reference set point across the load (V_{ncref}). This way the power consumption (both active and reactive in case of non-unity power factor load) of the load increases to regulate the PoC voltage back to its reference value.

$$\left[\Delta\dot{x_{21}}\right] = \left[0\right]\left[\Delta x_{21}\right] + \begin{bmatrix}\frac{V_{pocd0}}{V_{pocmag0}} & \frac{V_{pocq0}}{V_{pocmag0}}\end{bmatrix}\begin{bmatrix}\Delta V_{pocd}\\ \Delta V_{pocq}\end{bmatrix} \tag{11}$$

$$\left[\Delta V_{ncref}\right] = \left[k_{iv}\right]\left[\Delta x_{21}\right] + \begin{bmatrix}\frac{k_{pv}V_{pocd0}}{V_{pocmag0}} & \frac{k_{pv}V_{pocq0}}{V_{pocmag0}}\end{bmatrix}\begin{bmatrix}\Delta V_{pocd}\\ \Delta V_{pocq}\end{bmatrix} \tag{12}$$

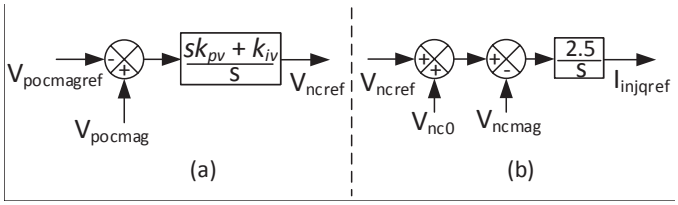

Figure 8. Block diagram of (a) PoC and (b) load voltage control loops

The state variable associated with the inner loop is denoted by Δx_{22}. The outer loop sets the reference for the inner loop which is updated by the maximum load voltage V_{nc0}, (i.e. minimum voltage across the filter capacitor) corresponding to the operating point $V_{pocmag0}$. A minimum voltage is required across the filter capacitor to ensure satisfactory operation of the PLL. The minimum filter capacitor voltage is considered to be 50 V in this study. The tuning of the PLL is carried out considering this minimum voltage. The choice of 50V is prompted by the fact that a sufficiently high value would ease the tuning of the PLL parameters to achieve an acceptable dynamic response. However, in practice this minimum filter voltage can be well below 50V depending on the type of PLL and the tuning of its compensator.

For a resistive load, $V_{nc0} = \sqrt{V_{pocmag0}^2 - 50^2}$ which is linearized as before and is expressed as $\frac{V_{pocd0}}{\sqrt{V_{pocmag0}^2-50^2}}\Delta V_{pocd}$ for an incremental change in $d-$ axis component. Similar expression can be obtained for an incremental change in the $q-$axis component. The load voltage magnitude feedback term V_{ncmag} is also linearized in a similar way around V_{ncmag0}. The SSM of the inner loop (Fig. 8 (b)) is given by (13) and (14). In (14) (and other equations henceforth), zero in bold letter denote a matrix of appropriate dimension.

$$\left[\Delta\dot{x_{22}}\right] = \left[0\right]\left[\Delta x_{22}\right] + \begin{bmatrix}1\\ \frac{-V_{ncd0}}{V_{ncmag0}}\\ \frac{-V_{ncq0}}{V_{ncmag0}}\\ \frac{V_{pocd0}}{\sqrt{V_{pocmag0}^2-50^2}}\\ \frac{V_{pocq0}}{\sqrt{V_{pocmag0}^2-50^2}}\end{bmatrix}^T\begin{bmatrix}\Delta V_{ncref}\\ \Delta V_{ncd}\\ \Delta V_{ncq}\\ \Delta V_{pocd}\\ \Delta V_{pocq}\end{bmatrix} \tag{13}$$

$$\left[\Delta I_{injqref}\right] = \left[2.5\right]\left[\Delta x_{22}\right] + \left[\mathbf{0}\right]\begin{bmatrix}\Delta V_{ncref}\\ \Delta V_{ncd}\\ \Delta V_{ncq}\\ \Delta V_{pocd}\\ \Delta V_{pocq}\end{bmatrix} \tag{14}$$

C. Current Control Loop

The structure of the current control loop adopted here is standard for any power electronic converter. The state variables associated with the PI controllers in d and q axis loops are denoted by $\Delta\gamma_d$ and $\Delta\gamma_q$, respectively and the controller gains (same for d and q axis loops) are k_{pc} and k_{ic}. The SSM of the current controller is given by (15) and (16). The incremental changes in the current control loop reference

This article has been accepted for publication in a future issue of this journal, but has not been fully edited. Content may change prior to final publication. Citation information: DOI 10.1109/TSG.2017.2772224, IEEE Transactions on Smart Grid

values are denoted by $\Delta I_{injdref}$ & $\Delta I_{injqref}$ while the change in the inverter currents and filter voltages are expressed as ΔI_{injd} & ΔI_{injq} and ΔV_{esd} & ΔV_{esq}, respectively.

$$\begin{bmatrix}\Delta\dot{\gamma}_d\\ \Delta\dot{\gamma}_q\end{bmatrix} = [\mathbf{0}]\begin{bmatrix}\Delta\gamma_d\\ \Delta\gamma_q\end{bmatrix} + \begin{bmatrix}1 & 0\\ 0 & 1\\ -1 & 0\\ 0 & -1\\ 0 & 0\\ 0 & 0\end{bmatrix}^T \begin{bmatrix}\Delta I_{injdref}\\ \Delta I_{injqref}\\ \Delta I_{injd}\\ \Delta I_{injq}\\ \Delta V_{esd}\\ \Delta V_{esq}\end{bmatrix} \tag{15}$$

$$\begin{bmatrix}\Delta V_{invd}\\ \Delta V_{invq}\end{bmatrix} = \begin{bmatrix}k_{ic} & 0\\ 0 & k_{ic}\end{bmatrix}\begin{bmatrix}\Delta\gamma_d\\ \Delta\gamma_q\end{bmatrix} + \begin{bmatrix}k_{pc} & 0\\ 0 & k_{pc}\\ -k_{pc} & \omega_0 L_f\\ -\omega_0 L_f & -k_{pc}\\ 1 & 0\\ 0 & 1\end{bmatrix}^T \begin{bmatrix}\Delta I_{injdref}\\ \Delta I_{injqref}\\ \Delta I_{injd}\\ \Delta I_{injq}\\ \Delta V_{esd}\\ \Delta V_{esq}\end{bmatrix} \tag{16}$$

D. Filter

The SSM of the filter part of the ES can be obtained from the dynamics of the inverter current (I_{inj}) and filter capacitor voltage (V_{es}) given by (1), (2), (3) and (4). The state variables are the $d-$ and $q-$ axis components of the inverter current (I_{injd}, I_{injq}) and the filter capacitor voltage (V_{esd}, V_{esq}). The equations are linearized around I_{injd0}, V_{esd0} (and similarly for the $q-$ axis) to derive the SSM of the filter as in (17) and (18). The filter resistance, inductance and capacitance are given by R_f, L_f and C_f, the load resistance is given by R_{NC} and ω_0 denotes the nominal frequency of the network.

$$\begin{bmatrix}\dot{\Delta I_{injd}}\\ \dot{\Delta I_{injq}}\\ \dot{\Delta V_{esd}}\\ \dot{\Delta V_{esq}}\end{bmatrix} = \begin{bmatrix}-\frac{R_f}{L_f} & \omega_0 & -\frac{1}{L_f} & 0\\ -\omega_0 & -\frac{R_f}{L_f} & 0 & -\frac{1}{L_f}\\ \frac{1}{C_f} & 0 & 0 & \omega_0\\ 0 & \frac{1}{C_f} & -\omega_0 & 0\end{bmatrix}\begin{bmatrix}\Delta I_{injd}\\ \Delta I_{injq}\\ \Delta V_{esd}\\ \Delta V_{esq}\end{bmatrix} + \begin{bmatrix}I_{injq0} & \frac{1}{L_f} & 0 & 0 & 0\\ -I_{injd0} & 0 & \frac{1}{L_f} & 0 & 0\\ V_{esq0} & 0 & 0 & \frac{1}{C_f R_{NC}} & 0\\ -V_{esd0} & 0 & 0 & 0 & \frac{1}{C_f R_{NC}}\end{bmatrix}\begin{bmatrix}\Delta\omega\\ \Delta V_{invd}\\ \Delta V_{invq}\\ \Delta V_{ncd}\\ \Delta V_{ncq}\end{bmatrix} \tag{17}$$

$$\begin{bmatrix}\Delta I_{injd}\\ \Delta I_{injq}\\ \Delta V_{esd}\\ \Delta V_{esq}\end{bmatrix} = \begin{bmatrix}1 & 0 & 0 & 0\\ 0 & 1 & 0 & 0\\ 0 & 0 & 1 & 0\\ 0 & 0 & 0 & 1\end{bmatrix}\begin{bmatrix}\Delta I_{injd}\\ \Delta I_{injq}\\ \Delta V_{esd}\\ \Delta V_{esq}\end{bmatrix} + [\mathbf{0}]\begin{bmatrix}\Delta\omega\\ \Delta V_{invd}\\ \Delta V_{invq}\\ \Delta V_{ncd}\\ \Delta V_{ncq}\end{bmatrix} \tag{18}$$

E. Network and Loads

The simple network shown in Fig. 5 with three segments and an ES is considered here. The load R_{new} used for creating disturbance is modelled as a current source I_s with a high resistance (R_{high}) in parallel. The transformer impedance (R_{tr} and L_{tr}) is merged within R_1 and L_1 in (19) and (20). The line resistance R_3 is merged with the equivalent load (R_C) while the inductance L_3 is neglected. The state variables are the $d-$ and $q-$ axis components of the line currents flowing through L_1 and L_2. The SSM of the network and the load is given by (21) and (22) with A_{line}, B_{line}, C_{line} and D_{line} expressed as in (19), (20), (23) and (24). The incremental change in the source voltage (and the disturbance current) is denoted by ΔV_{sd} & ΔV_{sq} (ΔI_{sd} & ΔI_{sq}).

$$\begin{bmatrix}\dot{\Delta I_{L1d}}\\ \dot{\Delta I_{L1q}}\\ \dot{\Delta I_{L2d}}\\ \dot{\Delta I_{L2q}}\end{bmatrix} = A_{line}\begin{bmatrix}\Delta I_{L1d}\\ \Delta I_{L1q}\\ \Delta I_{L2d}\\ \Delta_{L2q}\end{bmatrix} + B_{line}\begin{bmatrix}\Delta\omega\\ \Delta V_{sd}\\ \Delta V_{sq}\\ \Delta I_{sd}\\ \Delta I_{sq}\\ \Delta V_{esd}\\ \Delta V_{esq}\end{bmatrix} \tag{21}$$

$$\begin{bmatrix}\Delta I_{L1d}\\ \Delta I_{L1q}\\ \Delta I_{L2d}\\ \Delta I_{L2q}\\ \Delta I_d\\ \Delta I_q\end{bmatrix} = C_{line}\begin{bmatrix}\Delta I_{L1d}\\ \Delta I_{L1q}\\ \Delta I_{L2d}\\ \Delta_{L2q}\end{bmatrix} + D_{line}\begin{bmatrix}\Delta\omega\\ \Delta V_{sd}\\ \Delta V_{sq}\\ \Delta I_{sd}\\ \Delta I_{sq}\\ \Delta V_{esd}\\ \Delta V_{esq}\end{bmatrix} \tag{22}$$

$$C_{line} = \begin{bmatrix}1 & 0 & 0 & 0\\ 0 & 1 & 0 & 0\\ 0 & 0 & 1 & 0\\ 0 & 0 & 0 & 1\\ 0 & 0 & \frac{R_C}{R_C+R_{NC}} & 0\\ 0 & 0 & 0 & \frac{R_C}{R_C+R_{NC}}\end{bmatrix} \tag{23}$$

$$D_{line} = \begin{bmatrix}0 & 0 & 0 & 0 & 0 & 0\\ 0 & 0 & 0 & 0 & 0 & 0\\ 0 & 0 & 0 & 0 & 0 & 0\\ 0 & 0 & 0 & 0 & 0 & 0\\ 0 & 0 & 0 & 0 & -\frac{1}{R_C+R_{NC}} & 0\\ 0 & 0 & 0 & 0 & 0 & -\frac{1}{R_C+R_{NC}}\end{bmatrix} \tag{24}$$

Once the SSM is developed for the individual sub-systems (9)-(24), their A, B, C, D matrices are arranged together to form block-diagonal matrices. As an example, for four sub-systems, a block-diagonal state matrix $A = diag(A_1, A_2, A_3, A_4)$ is formed (and similarly for B, C, D matrices). Further, a matrix L_T is formed to capture the algebraic relationship between the inputs and outputs of all the subsystems. Finally, the state matrix of the whole system (F) is computed as (25). More details of this Component Connection Method (CCM) can be found in [18].

$$F = A + BL_T(I - DL_T)C^{-1} \tag{25}$$

The SSM for a simple network with one ES can be easily scaled up to include any number of network segments and ESs using CCM by simply repeating the equations for individual subsystems. This is used for the study case discussed next

This article has been accepted for publication in a future issue of this journal, but has not been fully edited. Content may change prior to final publication. Citation information: DOI 10.1109/TSG.2017.2772224, IEEE Transactions on Smart Grid

in Section IV where four network segments and two ESs are considered, as shown in Fig. 10.

Presence of more than one converter requires that all the variables are expressed in a common reference frame. This is achieved by the frame transformation method provided in [20]. As an example, the filter voltage V_{es} can be expressed on a common reference frame 'DQ' according to (26), where T_S and T_C are the transformation matrices given by (27) & (28) and $\Delta\delta$ is the incremental change in the phase angle difference between the reference frame of the respective inverter and the common reference frame 'DQ'. In (27) & (28), V_{esd0}, V_{esq0} & δ_0 represent the corresponding values at a stable operating point.

$$\begin{bmatrix}\Delta V_{esD}\\ \Delta V_{esQ}\end{bmatrix} = T_S \begin{bmatrix}\Delta V_{esd}\\ \Delta V_{esq}\end{bmatrix} + T_C \begin{bmatrix}\Delta\delta\end{bmatrix} \tag{26}$$

$$T_S = \begin{bmatrix} cos(\delta_0) & -sin(\delta_0)\\ sin(\delta_0) & cos(\delta_0)\end{bmatrix} \tag{27}$$

$$T_C = \begin{bmatrix} -V_{esd0}sin(\delta_0) - V_{esq0}cos(\delta_0)\\ V_{esd0}cos(\delta_0) - V_{esq0}sin(\delta_0)\end{bmatrix} \tag{28}$$

F. Validation of Linearized State Space model

The developed SSM is validated by comparing the dynamic response of the state variables with respect to that of the non-linear model developed in Matlab Simulink. At $t = 1$sec, a 100 W disturbance was introduced through R_{new} (Fig. 5) for 3 cycles. Fig. 9 shows the comparison for six state variables associated with the filter capacitor and the network inductances. The responses match closely confirming the validity of the SSM.

IV. Frequency-domain Analysis

The modelling framework discussed in Section III is used to obtain the SSM of the study system shown in Fig. 10. The dq-frame corresponding to the first electric spring (ES1) is considered to be the common frame and all other quantities are referred to this using the previously discussed transformation technique (26), (27) & (28).

Eigen value analysis of the state matrix (25) of the study system shown in Fig. 10 confirms that there are 32 state variables. There are two high-frequency modes of 472.31 Hz & 369.63 Hz and a third mode (56.07 Hz) close to the fundamental frequency. Participation factor analysis reveals that the filter capacitor voltage of both ESs (V_{es1} & V_{es2}) and the current through the network segment 1 (I_{L1}) and 2 (I_{L2}) have dominant participation in the two high-frequency modes (472.31 Hz & 369.63 Hz) while the 56.07 Hz mode is mainly associated with the filter capacitor voltage.

Varying the network parameters, such as the length of the line segments and R/X ratio, over a certain range shows movement of the critical system modes obtained from the eigen values of the system state matrix. This study helps to ascertain the overall small signal stability of the system under different scenarios. Although the study system shown in Fig. 10 is simple, varying the length of line segments 1, 2 and 3 and the R/X ratios cover a wide range of distribution network scenarios. For instance, the length of line segment 1 and 2 indicates the location of the ES with respect to the substation while the length of line segment 3 signifies the proximity of adjacent ESs. Similarly, a range of R/X ratio can be chosen to represent a dense urban ($R/X \approx 4$) to sparse rural ($R/X \approx 10$) low-voltage (LV) network as well as the medium-voltage (MV) level ($R/X \approx 1$) with industrial/commercial customers.

Stability of the distribution network with ES (inverter in series with the customer load) is compared against the case where PoC voltage is regulated by shunt (connection with respect to the customer load) converters such as STATCOM or DG inverters. The inverters in both cases are chosen to be equivalent in terms of PoC voltage regulation capability. The SSM of the network with DG inverters is fairly well reported and hence, not included in this paper. The readers can refer to [9] for details. The SSM of the study system shown in Fig. 10, but with the two ESs replaced by equivalent DG inverters, reveals the presence of four modes with frequencies of 4798.3Hz, 4695Hz, 1124.46Hz and 996.23Hz which are much higher than the case with ES.

A. Distance from Substation

The impact of distance of the ES or shunt converter from the substation is investigated by varying the length of line segments 1 and 2 which are separated by a unity power factor

$$A_{line} = \begin{bmatrix} -\frac{R_1+R_{high}}{L_1} & \omega_0 & \frac{R_{high}}{L_1} & 0\\ -\omega_0 & -\frac{R_1+R_{high}}{L_1} & 0 & \frac{R_{high}}{L_1}\\ \frac{R_{high}}{L_2} & 0 & -\frac{1}{L_2}(R_2+R_{high}+\frac{R_{NC}R_C}{R_{NC}+R_C}) & \omega_0\\ 0 & \frac{R_{high}}{L_2} & -\omega_0 & -\frac{1}{L_2}(R_2+R_{high}+\frac{R_{NC}R_C}{R_{NC}+R_C})\end{bmatrix} \tag{19}$$

$$B_{line} = \begin{bmatrix} I_{L1q0} & \frac{1}{L_1} & 0 & -\frac{R_{high}}{L_1} & 0 & 0 & 0\\ -I_{L1d0} & 0 & \frac{1}{L_1} & 0 & -\frac{R_{high}}{L_1} & 0 & 0\\ I_{L2q0} & 0 & 0 & \frac{R_{high}}{L_2} & 0 & -\frac{1}{L_2}\frac{R_C}{R_C+R_{NC}} & 0\\ -I_{L2d0} & 0 & 0 & 0 & \frac{R_{high}}{L_2} & 0 & -\frac{1}{L_2}\frac{R_C}{R_C+R_{NC}}\end{bmatrix} \tag{20}$$

This article has been accepted for publication in a future issue of this journal, but has not been fully edited. Content may change prior to final publication. Citation information: DOI 10.1109/TSG.2017.2772224, IEEE Transactions on Smart Grid

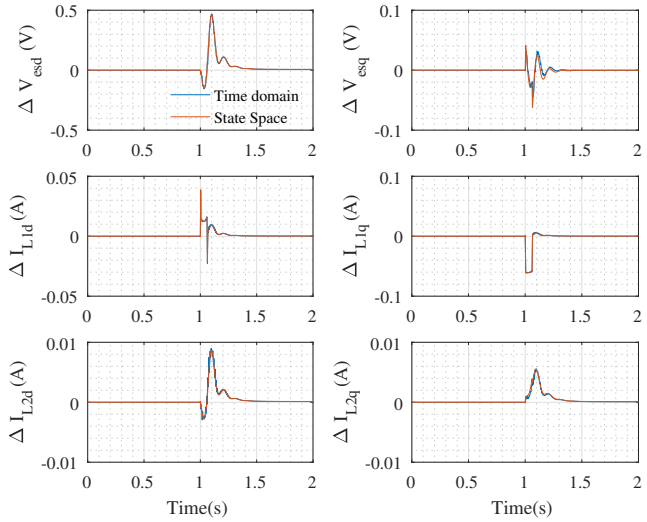

Figure 9. Comparison of dynamic response of state variables in linearized state space model and non-linear model due to a small disturbance

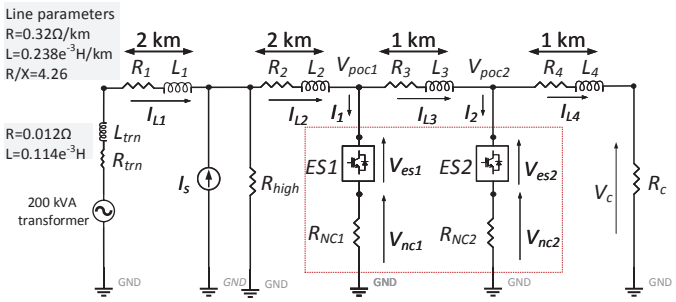

Figure 10. Study system with two ESs used for frequency-domain analysis

load. The length of the remaining line segments are kept the same as the base case (as in Fig. 10) and the R/X ratio of all segments are fixed at 4.26. The impact of varying the lengths between 0.1km to 2km on the 472.31Hz & 369.63 Hz modes is shown in Fig. 11(a) for ES. The frequency of both modes is significantly higher for ESs located farther away from the substation. However, the real part remains well beyond $-4000s^{-1}$ (i.e. far away in the left half of s-plane) without posing any threat to network stability.

Fig. 11(b) shows the impact with ESs replaced by equivalent DG inverters. In this case, increasing distance from the substation causes the high frequency modes ($>$ 4 kHz) to move away from the imaginary axis. It is worth noting that with ES the modes are much farther away in the left half of the s-plane compared to the case with DG inverters.

B. Electrical Proximity

The length of line segment 3 is varied to represent the electrical proximity between adjacent ES or DG inverters. A single ES will typically be installed at the PoC of a cluster of customers instead of individual customers to exploit the load diversity. Depending on the number of customers within a cluster, the distance of separation between adjacent ESs will vary. Fig. 12(a) shows that separation distance has hardly any effect on the frequency of the mode while the real part remains beyond $-3500s^{-1}$, thus posing no threat to system stability.

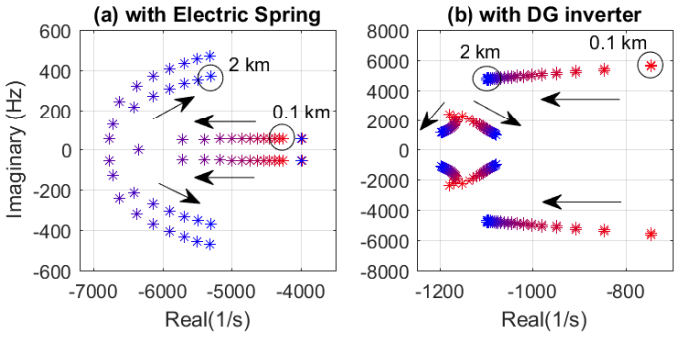

Figure 11. Root locus with (a) ES and (b) DG inverters when length of L1 & L2 is varied from 0.1km to 2km (red to blue) while keeping the other line parameters constant

Fig. 12(b) shows that DG inverters in close electrical proximity will result in very high frequency modes ($>$ 10 kHz). With increasing separation, the frequency reduces but the modes migrate closer to the imaginary axis.

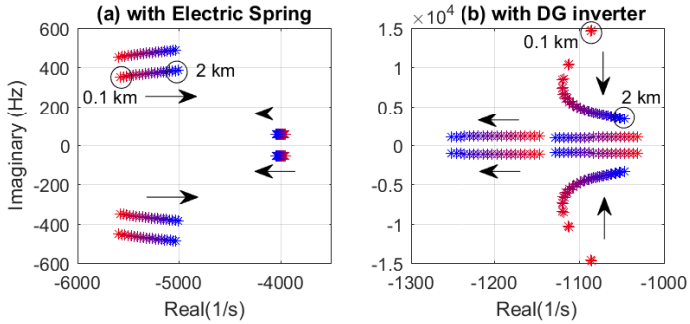

Figure 12. Root locus with (a) ES and (b) DG inverters when length of L3 is varied from 0.1km to 2km (red to blue) while keeping the other line parameters constant

C. Distribution Network Voltage Level

The R/X ratio of the line segments 1 and 2 is varied between 1 (MV level) to 10 (LV level-sparse rural network). The state variables associated with line segments 1 and 2 have dominant participation in the 472.31 Hz & 369.63 Hz modes present in the case of ES. This results in a large shift in those modes seen in Fig. 13(a). For higher R/X ratios, the modes move farther to left of the s-plane due to larger damping introduced by higher resistance. Similar effect is observed in Fig. 13(b) in case of DG inverter except that the frequencies increase slightly for higher R/X unlike the case with ES where it reduces slightly.

Fig. 14 shows the effect of varying the R/X ratio of line segment 3 while keeping other line parameters constant. The state variable associated with this line segment shows very limited impact on the three system modes (Fig. 14(a)) compared to varying the R/X of line segment 1 & 2 (Fig. 13(a)). For the case with DG inverter, varying the R/X ratio of line segment 3 actually shows movement of the high frequency mode whereas, limited movement is observed for the lower frequency mode compared to Fig. 13(b).

From the discussion in Sections IV-A, IV-B and IV-C, it can be concluded that the installation of ESs at different

This article has been accepted for publication in a future issue of this journal, but has not been fully edited. Content may change prior to final publication. Citation information: DOI 10.1109/TSG.2017.2772224, IEEE Transactions on Smart Grid

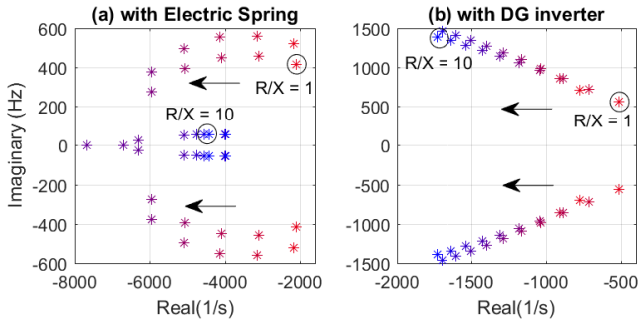

Figure 13. Root locus with (a) ES and (b) DG inverters when R/X ratios of L1 & L2 are varied from 1 to 10 (red to blue) while keeping the other line parameters constant

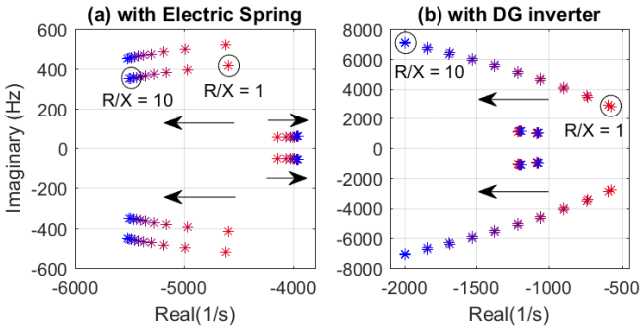

Figure 14. Root locus plot with (a) ES and (b) DG inverters when R/X ratio of L3 is varied from 1 to 10 (red to blue) while keeping the other line parameters constant

locations with respect to the substation, with varying electrical separation and at MV and LV levels will not pose any threat to distribution network stability. In fact, the situation is more stable (modes are farther to the left of s-plane) with ES than equivalent penetration of DG inverters. Unlike the case of a microgrid [9], the choice of voltage droop gain did not have a major influence on stability in this case due to the stiff (or strong) upstream system mimicked by the voltage source in Fig. 5 & 10.

The small signal analysis presented here is based on a simple network. However, it covers a wide range of scenarios encountered in practical distribution networks. For example, the impact of different distance of an ES from the substation is captured by varying the length of the line segments 1 and 2 while maintaining the R/X ratio and the length of other lines constant. Similarly, the impact of electrical proximity between adjacent ESs is investigated by varying the length of the line segment 3 while keeping the length and R/X ratio of other lines constant. Voltage level (e.g. MV or LV) and topology (e.g. dense urban, spare rural network) of distribution network is accounted for in the study by varying the R/X ratio of the line segments. The results presented in this section are thus extendible for the simulation study presented in the following section on a typical urban distribution network.

V. Simulation Study

The capability of a group of ES to regulate the PoC voltage is demonstrated on a typical urban distribution network adopted from [23]. There are four main feeders and several lateral feeders as shown in Fig. 15. The total load on the substation transformer (11.0.4 kV, 550 kVA) is 431.3 kW (at 1 p.u. voltage) which is equally divided among the residential customers. The feeder lengths and the rating of the load clusters are mentioned in Fig. 15 together with the cable type [23] for each segment.

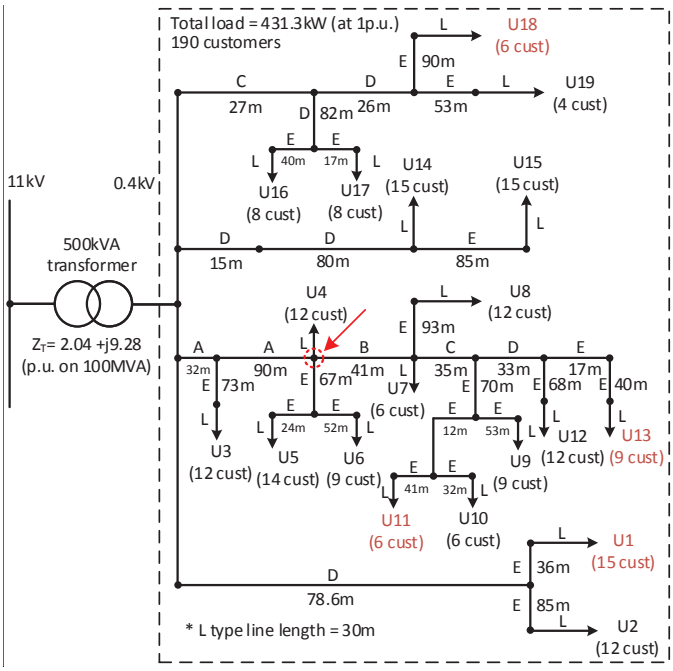

Figure 15. Low voltage network for simulation study [23]

For this study, load clusters U1, U11, U13 and U18 are each equipped with one ES each. An under-voltage disturbance is introduced at the location marked by an arrow in Fig. 15. This reduces the PoC voltages as shown in Fig. 16(a). The voltage injected by the ESs reduces the deviation in PoC voltage from the nominal value as shown in Fig. 16(b). This is achieved at the expense of reduced voltage across the loads which are still maintained within the stipulated limits. The ESs at U11 and U13 are unable to restore the PoC voltages back to the nominal value as their combined capacity is not adequate considering the severity of the voltage disturbance.

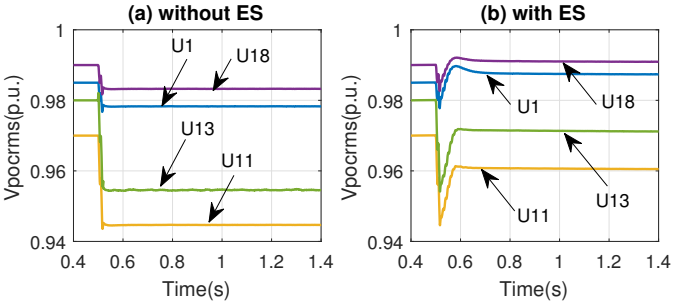

Figure 16. Variation of PoC voltage (a) without ES, (b) with ES

VI. Conclusion

This paper shows that Electric Springs installed in distribution networks are not likely to threaten the small signal stability of the system. In fact, the stability margin with ES

installed is more than the case with equivalent penetration of shunt converters such as DG inverters. The distance of an ES from the substation, proximity between adjacent ES installations and the R/X ratio of the distribution feeder influence the stability. However, for a wide range of distance, proximity and R/X ratios representing low- to medium (MV) voltage levels and typical dense urban networks to sparse rural feeders, the distribution network was found to be stable. The linearized state-space model of vector controlled ES presented in this paper could be incorporated into the stability models of microgrids to study how droop control of ES (required for appropriate sharing of voltage control burden [24]) impacts the overall stability.

REFERENCES

[1] S. Y. R. Hui, C. K. Lee, and F. F. Wu, "Electric springs - A new smart grid technology," *IEEE Transactions on Smart Grid*, vol. 3, no. 3, pp. 1552–1561, 2012.

[2] C. K. Lee, B. Chaudhuri, and S. Y. R. Hui, "Hardware and control implementation of electric springs for stabilizing future smart grid with intermittent renewable energy sources," *IEEE Journal of Emerging and Selected Topics in Power Electronics*, vol. 1, no. 1, pp. 18–27, 2013.

[3] X. Luo, Z. Akhtar, C. K. Lee, B. Chaudhuri, S. C. Tan, and S. Y. R. Hui, "Distributed voltage control with electric springs: Comparison with STATCOM," *IEEE Transactions on Smart Grid*, vol. 6, no. 1, pp. 209–219, 2014.

[4] D. Chakravorty, B. Chaudhuri, and S. Y. R. Hui, "Rapid frequency response from smart loads in great britain power system," *IEEE Transactions on Smart Grid*, vol. PP, no. 99, pp. 1–1, 2016.

[5] Y. Shuo, S. C. Tan, C. K. Lee, and S. Y. R. Hui, "Electric spring for power quality improvement," in *IEEE Applied Power Electronics Conference and Exposition (APEC)*, 2014, pp. 2140–2147.

[6] S. Yan, S. C. Tan, C. K. Lee, B. Chaudhuri, and S. Y. R. Hui, "Electric springs for reducing power imbalance in three-phase power systems," *IEEE Transactions on Power Electronics*, vol. 30, no. 7, pp. 3601–3609, July 2015.

[7] L. Liang, Y. Hou, D. Hill, and S. Y. R. Hui, "Enhancing resilience of microgrids with electric springs," *IEEE Transactions on Smart Grid*, vol. PP, no. 99, pp. 1–1, 2017.

[8] D. Chakravorty, B. Chaudhuri, and S. Y. R. Hui, "Estimation of aggregate reserve with point-of-load voltage control," *IEEE Transactions on Smart Grid*, vol. PP, no. 99, pp. 1–1, 2017.

[9] N. Bottrell, M. Prodanovic, and T. C. Green, "Dynamic stability of a microgrid with an active load," *IEEE Transactions on Power Electronics*, vol. 28, no. 11, pp. 5107–5119, Nov 2013.

[10] F. Andrn, B. Bletterie, S. Kadam, P. Kotsampopoulos, and C. Bucher, "On the stability of local voltage control in distribution networks with a high penetration of inverter-based generation," *IEEE Transactions on Industrial Electronics*, vol. 62, no. 4, pp. 2519–2529, April 2015.

[11] D. Chakravorty, Z. Akhtar, B. Chaudhuri, and S. Y. R. Hui, "Comparison of primary frequency control using two smart load types," in *2016 IEEE Power and Energy Society General Meeting (PESGM)*, July 2016, pp. 1–5.

[12] Z. Akhtar, B. Chaudhuri, and S. Y. R. Hui, "Smart loads for voltage control in distribution networks," *IEEE Transactions on Smart Grid*, vol. 8, no. 2, pp. 937–946, March 2017.

[13] N. R. Chaudhuri, C. K. Lee, B. Chaudhuri, and S. Y. R. Hui, "Dynamic modeling of electric springs," *IEEE Transactions on Smart Grid*, vol. 5, no. 5, pp. 2450–2458, 2014.

[14] Y. Yang, S. S. Ho, S. c. Tan, and S. Y. R. Hui, "Small-signal model and stability of electric springs in power grids," *IEEE Transactions on Smart Grid*, vol. PP, no. 99, pp. 1–1, 2017.

[15] A. Yazdani and R. Iravani, *Voltage-Sourced Converters in Power Systems*, 1st ed. John Wiley INC., 2010.

[16] J. Sun, "Impedance-based stability criterion for grid-connected inverters," *IEEE Transactions on Power Electronics*, vol. 26, no. 11, pp. 3075–3078, Nov 2011.

[17] A. Rygg and M. Molinas, "Real-time stability analysis of power electronic systems," in *2016 IEEE 17th Workshop on Control and Modeling for Power Electronics (COMPEL)*, June 2016, pp. 1–7.

[18] Y. Wang, X. Wang, F. Blaabjerg, and Z. Chen, "Small-signal stability analysis of inverter-fed power systems using component connection method," *IEEE Transactions on Smart Grid*, vol. PP, no. 99, pp. 1–1, 2017.

[19] Q. Huang and R. Kaushik, "An improved delayed signal cancellation pll for fast grid synchronization under distorted and unbalanced grid condition," *IEEE Transactions on Industry Applications*, vol. PP, no. 99, pp. 1–1, 2017.

[20] N. Pogaku, M. Prodanovic, and T. C. Green, "Modeling, analysis and testing of autonomous operation of an inverter-based microgrid," *IEEE Transactions on Power Electronics*, vol. 22, no. 2, pp. 613–625, March 2007.

[21] N. Kroutikova, C. a. Hernandez-Aramburo, and T. C. Green, "State-space model of grid-connected inverters under current control mode," *IET Electric Power Applications*, vol. 1, no. 3, pp. 329–338, May 2007.

[22] C. C. Chang, D. Gorinevsky, and S. Lall, "Dynamical and voltage profile stability of inverter-connected distributed power generation," *IEEE Transactions on Smart Grid*, vol. 5, no. 4, pp. 2093–2105, July 2014.

[23] Cigre Working Group C4.605, Rep.5, "Modeling and Aggregation of Loads in Flexible Power Networks," Tech. Rep., Feb. 2014.

[24] C. K. Lee, N. R. Chaudhuri, B. Chaudhuri, and S. Y. R. Hui, "Droop control of distributed electric springs for stabilizing future power grid," *IEEE Transactions on Smart Grid*, vol. 4, no. 3, pp. 1558–1566, 2013.

Diptargha Chakravorty (S'14) received the M.Tech degree in Energy Engineering in 2012 from Indian Institute of Technology Delhi, India. He has worked as a research assistant for a year with the Institute of Electrical Power Systems and High Voltage Engineering at the Technische Universitt Dresden, Germany. He is currently pursuing the Ph.D. degree from Imperial College London, U.K. His research interests include smart grid, demand side management, renewable energy integration and power quality.

Jinrui Guo (S'16) received the B.Sc. and M.Sc. degrees from North China Electric Power University, Beijing, China, in 2012 and 2015, respectively. He is currently pursuing the Ph.D. degree from Imperial College London, U.K. His research interests include power system stability, smart grid, and renewable energy integration.

Balarko Chaudhuri (M'06-SM'11) received the Ph.D. degree in Electrical and Electronic engineering from Imperial College London, London, U.K., in 2005 where he is currently a Reader in Power Systems at the Control and Power Research Group. His research interests include power systems stability, grid integration of renewables, HVDC, FACTS, demand response and smart grids. Dr Chaudhuri is an editor of the IEEE Transactions on Smart Grid and an associate editor of the IEEE Systems Journal and Elsevier Control Engineering Practice. He is a Fellow of the Institution of Engineering and Technology (IET) and a member of the International Council on Large Electric Systems (CIGRE).

Shu Yuen Ron Hui (M'87-SM'94-F'03) received the B.Sc. (Hons.) degree in Electrical and Electronic engineering from the University of Birmingham, Birmingham, U.K., in 1984, and the D.I.C. and Ph.D. degrees from Imperial College London, London, U.K., in 1987. He currently holds the Philip Wong Wilson Wong Chair Professorship with the University of Hong Kong, Hong Kong. Since 2010, he has concurrently held a part-time Chair Professorship in PowerElectronics at Imperial College London. He has published over 200 technical papers, including about 170 refereed journal publications and book chapters. Over 55 of his patents have been adopted by industry. Prof. Hui was the recipient of the IEEE Rudolf Chope Research and Development Award from the IEEE Industrial Electronics Society and the IET Achievement Medal (Crompton Medal) from the Institution of Engineering and Technology in 2010. He is a Fellow of the Australian Academy of Technological Sciences and Engineering. He is also the recipient of the 2015 IEEE William E. Newell Power Electronics Award. He is an Associate Editor of the IEEE TRANSACTIONS ON POWER ELECTRONICS and the IEEE TRANSACTIONS ON INDUSTRIALELECTRONICS.